Hexadirectional coding of visual space in human entorhinal cortex

Matthias Nau [1,2]*, Tobias Navarro Schröder[1,2], Jacob L. S. Bellmund[1,2] and Christian F. Doeller [1,2,3]*

Entorhinal grid cells map the local environment, but their involvement beyond spatial navigation remains elusive. We examined human functional MRI responses during a highly controlled visual tracking task and show that entorhinal cortex exhibited a sixfold rotationally symmetric signal encoding gaze direction. Our results provide evidence for a grid-like entorhinal code for visual space and suggest a more general role of the entorhinal grid system in coding information along continuous dimensions.

Grid cells in entorhinal cortex (EC) exhibit place-responsive firing patterns that represent self-location[1–4]. These firing patterns are sixfold rotationally symmetric (hexadirectional) and are implicated in navigation and the formation of maps of the local environment. Investigations in nonhuman primates show that EC neurons further encode eye-movement direction[5] and visual space[6]. Here grid cells fire as a function of gaze location rather than self-location, suggesting visuospatial coding in EC that is strikingly different from retinotopic representations typically found in visual cortex[7]. In humans, functional MRI (fMRI) has demonstrated that EC activity depends on virtual running direction in a hexadirectional manner, in line with a putative grid cell population response[8]. However, it is currently unknown whether human EC codes for visual space and eye movements beyond navigation.

We used fMRI to examine human EC responses during a visual tracking and object location memory task. Our experiment (Fig. 1 and Supplementary Figs. 1 and 2) ensured attentional focus on visuospatial information while balancing directional sampling of smooth-pursuit and saccadic eye movements. We exposed participants to a virtual arena from bird's eye view and presented a fixation target that moved within the environment in a highly controlled and directionally balanced fashion. We sampled eye movement directions with 10° angular resolution and monitored fixation accuracy with a magnetic resonance–compatible eye-tracking system. To facilitate spatial attention, participants memorized object locations within the environment (arena shown in two orientations: 0° and 180°) that were cued only when the fixation target crossed over them.

Imaging data were analyzed using a bootstrapping-based, leave-one-out threefold cross-validated symmetry test (see Methods). We fitted a general linear model to obtain beta estimates for each voxel and eye-movement direction for three data partitions (run blocks within which directional sampling was balanced) for every participant. For every EC voxel (Supplementary Fig. 3), we then estimated the phase of the putative six-peaked oscillatory modulation (putative grid orientation) of fMRI activity across directions, based on a normalized average of two of the data partitions. Using the third, independent, data partition, we then tested whether directions aligned to the putative grid orientation (0 modulo 60°) exhibited stronger EC activity than directions misaligned (30 modulo 60°) to it. This process was iterated until every data partition served as the test set once and as the training set twice. Using a bootstrapped distribution obtained by shuffling the direction labels of the test set 1,000 times, resulting contrast coefficients were transformed to z-scores, averaged across iterations and EC voxels and taken to the group level (Supplementary Fig. 4). Since the distribution of z-scores was non-normal (one-sample Kolmogorov–Smirnov goodness-of-fit test for EC: $K = 0.367$, $P = 5.2 \times 10^{-4}$), z-score we performed nonparametric one-sided Wilcoxon signed-rank tests to examine whether z-scores for aligned directions were systematically higher than for misaligned directions.

Eye-movement directions aligned to the putative grid orientation consistently induced stronger EC activity than misaligned directions ($z = 2.38$, $P = 8.7 \times 10^{-3}$; Fig. 2a). To investigate these results in more detail, we aligned each voxel's beta estimates, cross-validated before bootstrapping (also see Supplementary Fig. 5), to the respective estimated putative grid orientation and found that, across participants, the six aligned directions generally elicited stronger EC responses than the six misaligned directions (Fig. 2c). The hexadirectional effect in EC was therefore not driven by a single direction but rested upon a systematic sixfold rotational symmetry in response to eye movement direction. We repeated the main analysis for several control regions as well as biologically implausible control symmetries (Fig. 2d). Among all symmetries tested, and after Bonferroni correction, only sixfold symmetry yielded a significant modulation (control symmetries: fourfold: $z = 1.04$, $P = 0.150$; fivefold: $z = 0.43$, $P = 0.333$; sevenfold: $z = 1.12$, $P = 0.130$; eightfold: $z = 0.69$, $P = 0.245$). Among all control regions, and again after Bonferroni correction, only EC showed a significant hexadirectional modulation (control regions: early visual cortex: $z = 0.84$, $P = 0.200$; motor cortex: $z = -0.35$, $P = 0.635$; frontal lobe: $z = 1.08$, $P = 0.140$; parietal cortex: $z = 1.19$, $P = 0.117$). A subpart of the frontal lobe was weakly hexadirectionally modulated in line with previous studies[8,9] but did not survive Bonferroni correction (Supplementary Fig. 6). To examine whether EC generally responded to eye movements in our task irrespective of direction, we then compared responses to eye movements to a visual motion control in which the fixation target remained at the screen center while the arena moved instead, matching retinal motion in the main experiment (see Methods). Among our regions of interest (Fig. 2b), only early visual cortex ($z = 4.55$, $P = 5.3 \times 10^{-6}$) and parietal cortex ($z = -2.82$, $P = 4.8 \times 10^{-3}$), but not EC ($z = 1.50$, $P = 0.133$), exhibited significant responses in this contrast (Fig. 2d). EC hence did not respond to eye movements or to visual motion per se, but responded to gaze in a highly direction-specific fashion. We did not

[1]Kavli Institute for Systems Neuroscience, Centre for Neural Computation, The Egil and Pauline Braathen and Fred Kavli Centre for Cortical Microcircuits, NTNU, Norwegian University of Science and Technology, Trondheim, Norway. [2]Donders Institute for Brain, Cognition and Behaviour, Radboud University, Nijmegen, The Netherlands. [3]St. Olavs Hospital, Trondheim University Hospital, Trondheim, Norway. *e-mail: matthias.nau@ntnu.no; christian.doeller@ntnu.no

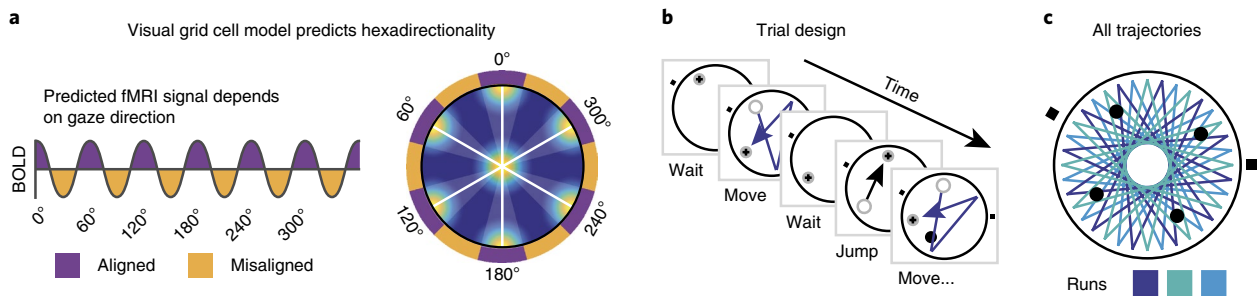**Fig. 1 | Hypothesis and task design. a**, Hypothesis. The number of firing fields crossed depends on eye movement direction (more fields are crossed for directions aligned to grid axes (white lines) compared to directions misaligned to it). Because grid orientation[3] and spatial phase[4] cluster across cells and because conjunctive direction-tuning has been reported to align to the grid axes[8], this relationship translates to hexadirectional biases of putative grid cell population activity, in turn predicting a stronger fMRI signal for aligned versus misaligned directions. BOLD, blood oxygen level–dependent contrast. **b**, Visual tracking task. Experiment consisted of 3 blocks of 3 runs incorporating 9 trials each. Each run tested a different set of 12 directions. Typical trial: each trial started with the fixation target (black cross) being stationary (1 s), then moving (6–10 s; blue arrows) to sample 3–5 eye-movement directions sequentially in 2-s blocks, followed by a waiting period (1 s) and finally jumping (black arrow) to a random position and continuing moving from there. Objects were shown when the fixation target moved over predefined locations (black circle). **c**, All trajectories tested in this experiment. Each run block tested all trajectories (36 directions) equally with 10° angular resolution. External landmarks: black squares. Objects were cued at four predefined locations, depicted as black circles.

find evidence for hexadirectional modulation in the visual motion control condition ($z = -0.39$, $P = 0.651$). Next, we estimated one putative grid orientation per voxel with maximized signal-to-noise ratio (direction-specific beta estimates averaged across partitions) and quantified how much these orientations varied across voxels, as well as around the participant's across-voxel mean orientation (Fig. 2e). We found that putative grid orientations were not random across voxels but clustered around the participant's mean orientation (V-test for nonuniformity, $V = 31.80$, $P = 3.46 \times 10^{-6}$), with higher coherence within compared to across hemispheres ($t_{28} = -3.67$, $P = 0.001$, confidence interval $[-0.03, -0.01]$; Supplementary Fig. 7). More specifically, voxels exhibiting a stronger hexadirectional signal varied less around the across-voxel mean than those showing a weaker effect ($t_{28} = -6.67$ $P = 1.5 \times 10^{-7}$, confidence interval $[-\infty, -0.19]$, also true for unsmoothed data; Supplementary Fig. 7). On the one hand, this indicates that not all EC voxels were engaged in our task (there is noise), but on the other hand it also indicates that others indeed represent activity with a predominant orientation. Consistent with previous reports of first-person navigation in nonpolarized environments[8], putative grid orientations were not clustered across participants (Rayleigh's tests for nonuniformity, arena orientation 1: $z = 0.083$, $P = 0.922$; orientation 2: $z = 0.141$, $P = 0.871$; see Methods). Participants were able to report all object locations equally well both from the bird's eye view ($F_{3,81} = 0.64$, $P = 0.593$) and in subsequent first-person navigation ($F_{3,81} = 1.9$, $P = 0.136$; Supplementary Fig. 2). Eye tracking analysis did not reveal any confounding symmetry in fixation accuracy relevant to our imaging results ($F_{4,92} = 1.7$, $P = 0.156$), and average eye velocity matched the one of the fixation targets equally well for all directions ($F_{35, 805} = 1.1$, $P = 0.313$; see Methods and Supplementary Fig. 8).

Our results provide (to our knowledge) the first evidence of gaze-dependent hexadirectional signals in human EC and are consistent with reports of eye-movement direction encoding[5] and visuospatial grid cells[6] in (nonhuman) primates. In contrast to the aforementioned studies, our experiment involved both smooth-pursuit and (low-amplitude) saccadic eye movements; however, it allowed us to examine eye movements with predominant directions (critical for our analysis), was highly controlled and had balanced sampling across directions, and reduced perceptual distortion effects known to occur in (high-amplitude) saccades[10]. Gaze location has been shown to drive spatial view cells in monkey hippocampus[11], and primates generally rely strongly on vision as they explore space[12]. While such hippocampal viewing responses have not yet been

reported in rodents, the hippocampal formation has been shown to integrate visual information[13]. In contrast to retinotopic[7] and spatiotopic[14,15] representations typically found in visual cortex, however, our results implicate human EC in encoding visual space with a grid-like code, a representation drastically different from any found in visual cortex, as well as from visually driven responses[16] and memory-guided visual processing[17] in other mediotemporal lobe regions. One alternative explanation for our results could be that participants imagine themselves navigating as they track the fixation disc. While hexadirectional signals have been observed during mental imagery[18], our results are unlikely to be explained in the same manner because, in contrast to the aforementioned study, our experiment engaged participants in an active attention task and because EC was not hexadirectionally modulated in the visual motion control. While saccade-direction cells[5] exhibiting hexa-directional population activity could provide a potential nongrid explanation of our results, such asymmetries in saccade-direction tuning have not yet been observed. However, grid cell population responses can provide a parsimonious yet substantiated explanation for the signal we observed (Fig. 1a). It remains to be shown how eye-movement-invariant visuospatial information reaches EC, as many areas contribute to visual constancy during eye movements[14]. However, given its strong involvement in visuospatial processing in both monkeys and humans[14,15], and despite not being hexadirec-tionally modulated in our task, parietal cortex appears to be a prime candidate for future studies in this context.

Recent reports implicate EC in coding not spatial information per se, but generally continuous feature dimensions also including sound frequency[19] or abstract knowledge[9]. The present study supports this notion and further suggests a domain-general coding regime in EC that is also employed to encode visual space and potentially contributes to memory-guided viewing behavior orchestrated by the hippocampal formation[20]. Our results are in line with reports of hexadirectional signals during virtual navigation[8] and mental simulation[18] and show that eye movement and visual information is processed in human EC. They further suggest a grid-like code for representing visual space and point toward a broader role of EC in cognition beyond spatial navigation[9,19].

Methods

Methods, including statements of data availability and any associated accession codes and references, are available at https://doi.org/10.1038/s41593-017-0050-8.
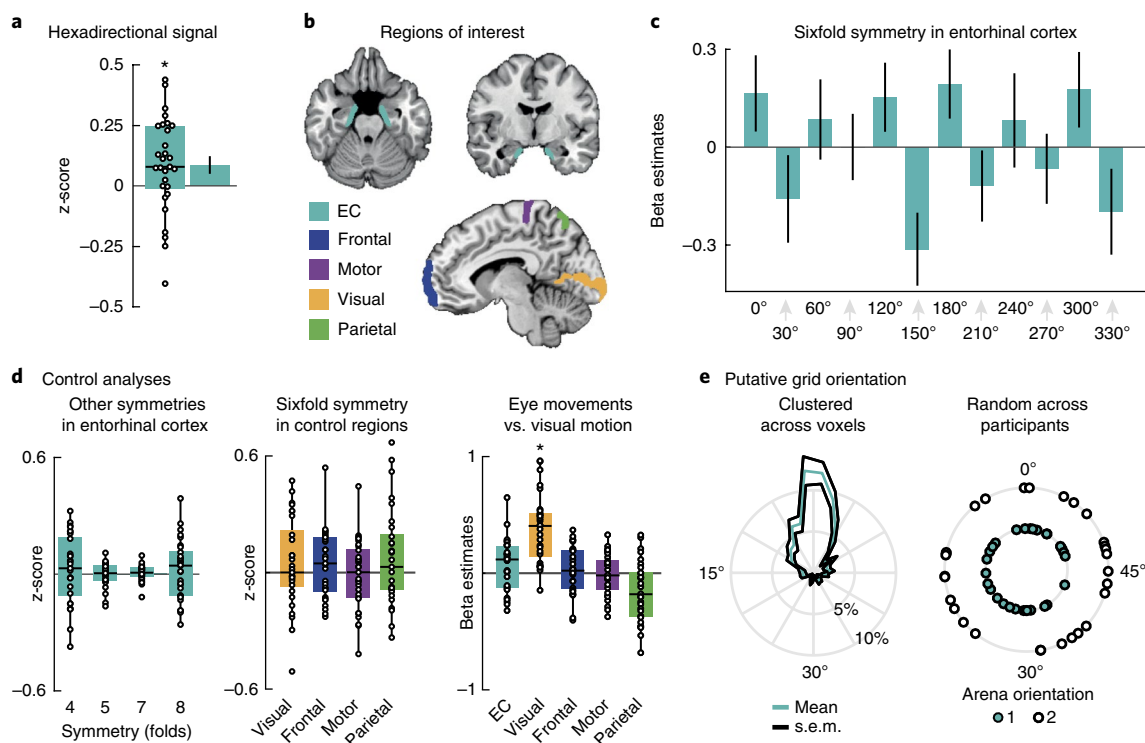
Fig. 2 | Gaze-dependent hexadirectional coding in EC. a, EC exhibited higher fMRI activity for aligned vs. misaligned directions (Bonferroni-corrected one-sided Wilcoxon signed-rank test, $z = 2.38$, $*P = 8.7 \times 10^{-3}$, $n = 29$). Left: aligned vs. misaligned contrast for single-participant data overlaid on whisker-and-box plots (center, median; box, 25th to 75th percentiles; whiskers, $1.5 \times$ interquartile range) and mean and s.e.m. across participants. Right: same data depicted as a bar plot, showing mean and s.e.m. across participants. **b**, Regions of interest (ROIs) displayed on the T1 template (Montreal Neurological Institute (MNI) coordinates: $X = -8$, $Y = -11$, $Z = -20$). **c**, To visualize the effect in **a** in more detail, we plot cross-validated beta estimates for aligned and misaligned directions, sorted according to putative grid orientation ($0°$). Each bar represents an averaged $20°$ bin of eye-movement directions averaged across the three iterations and across participants (see Methods). Error bars depict s.e.m. across 29 participants. **d**, Control analyses. Left: aligned vs. misaligned contrast for control symmetries (four-, five-, seven- and eightfold periodicity). Middle: sixfold symmetry effect for control regions. Right: eye movements vs. visual motion contrast. Activity in early visual cortex ($z = 4.55$, $*P = 5.3 \times 10^{-6}$) and parietal cortex ($z = -2.82$, $*P = 4.8 \times 10^{-3}$) was significantly different in these conditions (Bonferroni-corrected two-sided Wilcoxon signed-rank tests, $n = 29$). As in **a**, we plot single-participant data overlaid on whisker-and-box plots. **e**, Left: circular distances between putative grid orientation of each voxel and the circular mean across voxels; radial axes represent percent of voxels. Right: putative grid orientations across participants for both arena orientations.

References

1. Hafting, T., Fyhn, M., Molden, S., Moser, M.-B. & Moser, E. I. *Nature* **436**, 801–806 (2005).
2. Jacobs, J. et al. *Nat. Neurosci.* **16**, 1188–1190 (2013).
3. Stensola, H. et al. *Nature* **492**, 72–78 (2012).
4. Heys, J. G., Rangarajan, K. V. & Dombeck, D. A. *Neuron* **84**, 1079–1090 (2014).
5. Killian, N. J., Potter, S. M. & Buffalo, E. A. *Proc. Natl. Acad. Sci. USA* **112**, 15743–15748 (2015).
6. Killian, N. J., Jutras, M. J. & Buffalo, E. A. *Nature* **491**, 761–764 (2012).
7. Wandell, B. A., Dumoulin, S. O. & Brewer, A. A. *Neuron* **56**, 366–383 (2007).
8. Doeller, C. F., Barry, C. & Burgess, N. *Nature* **463**, 657–661 (2010).
9. Constantinescu, A. O., O'Reilly, J. X. & Behrens, T. E. J. *Science* **352**, 1464–1468 (2016).
10. Ross, J., Morrone, M. C., Goldberg, M. E. & Burr, D. C. *Trends Neurosci.* **24**, 113–121 (2001).
11. Rolls, E. T. *Hippocampus* **9**, 467–480 (1999).
12. Ekstrom, A. D. *Hippocampus* **25**, 731–735 (2015).
13. Chen, G., King, J. A., Burgess, N. & O'Keefe, J. *Proc. Natl. Acad. Sci. USA* **110**, 378–383 (2013).
14. Klier, E. M. & Angelaki, D. E. *Neuroscience* **156**, 801–818 (2008).
15. Kravitz, D., Saleem, K., Baker, C. & Mishkin, M. *Nat. Rev. Neurosci.* **12**, 217–230 (2011).
16. Epstein, R. & Kanwisher, N. *Nature* **392**, 598–601 (1998).
17. Summerfield, J. J., Lepsien, J., Gitelman, D. R., Mesulam, M. M. & Nobre, A. C. *Neuron* **49**, 905–916 (2006).
18. Bellmund, J. L. S., Deuker, L., Navarro Schröder, T. & Doeller, C. F. *eLife* https://doi.org/10.7554/eLife.16534 (2016).
19. Aronov, D., Nevers, R. & Tank, D. W. *Nature* **543**, 719–722 (2017).
20. Voss, J. L., Bridge, D. J., Cohen, N. J. & Walker, J. A. *Trends Cogn. Sci.* **21**, 577–588 (2017).

Author contributions

M.N., T.N.S., J.L.S.B. and C.F.D. designed the study; M.N. ran the experiments and analyzed the data; M.N. and C.F.D. wrote the manuscript; and all authors discussed the results and revised the manuscript.

Competing interests

The authors declare no competing financial interests.

Additional information

Supplementary information is available for this paper at https://doi.org/10.1038/s41593-017-0050-8.

Reprints and permissions information is available at www.nature.com/reprints.

Correspondence and requests for materials should be addressed to M.N. or C.F.D.

Publisher's note: Springer Nature remains neutral with regard to jurisdictional claims in published maps and institutional affiliations.

Methods

Participants. A total of 36 participants (22 female, age range: 18–35, normal or corrected to normal vision) were recruited for this study via the Radboud University Nijmegen online recruitment system. Participants were not grouped and hence no sample randomization or blinding was performed. Two participants were excluded due to strong head movements, frequently larger than the voxel size of 2 mm. Another 5 participants were excluded because eye tracking revealed low tracking-task performance (deviating more than one s.d. from the average fixation error across participants). In total, 29 participants entered the analysis (in line with a priori G*Power sample size estimation (https://stats.idre.ucla.edu/other/gpower) at 80% power, alpha = 0.05 and assumed medium effect size of d = 0.5, n = 27 participants; see the Life Sciences Reporting Summary for more information). The study was approved by the local ethics committee (CMO Arnhem-Nijmegen, The Netherlands), all relevant ethical regulations were followed, and participants gave written consent before the experiment.

Stimulus and experimental procedure. Prior to scanning, participants navigated a circular virtual arena (generated with Unreal Engine 2, https://www.unrealengine.com) in first-person perspective for 2–3 min (Supplementary Fig. 2c). During scanning we then exposed them to the same virtual arena from bird's eye view (screen size: 24° × 18°, arena diameter: 17° visual angle, Supplementary Fig. 2a) and presented a fixation target that moved within the environment in a highly controlled yet (to the participant) unknown fashion (fixation task). In addition, participants memorized object locations within the environment (object location memory task), for which the arena was shown in two orientations (0° and 180°) to enhance spatial attention. Stimuli were presented using Psychophysics Toolbox version 3 (http://psychtoolbox.org/). Arena orientation alternated across trials of each condition, which were presented in counterbalanced order. The arena was surrounded by two landmarks (two white squares matched in brightness, one hollow and one filled, at 0° and 150° relative to horizontal axis in orientation 1). Landmark identity alternated between the two locations across participants. The experiment consisted of a total of 9 runs with 9 trials each. To ensure a balanced sampling of directions, the first trial of each run was discarded. For every run, 4 trials of the main experiment (~1 min each) and 4 trials of visual motion control (~30 s each) were included in the analysis. Condition sequence was counterbalanced. At the end of the experiment, participants navigated the virtual environment in first-person view again (Supplementary Fig. 2c) and reported object locations by navigating to them and confirming the location via button press (25 trials, 6 trials per object, counterbalanced order, first trial was discarded).

Fixation task. Participants fixated at a fixation target (black cross on light gray circle, diameter: 0.8° visual angle) moving with a constant speed of 7.5°/s inside the arena, which was shown from a bird's eye view (Fig. 1 and Supplementary Figs. 1 and 2). The total trajectory of the fixation target resembled a twelve-pointed star (diameter: 15° visual angle from one point to another) and incorporated 12 directions in steps of 30°. In every trial, this trajectory, and hence each of the 12 directions, was tested twice and in blocks of 2 s each. To disrupt periodicity of the stimulus, we split the trajectory of each trial into 6 paths, whose presentation order was randomized. The path lengths varied from 3 to 5 path segments (movement of the fixation target from one point to the other and hence a 2-s long block of a given direction). After every 3–5 path segments, the fixation target stopped for 1 s, jumped to another randomly chosen point, paused another 1.5 s to facilitate successful fixation and then continued its movement from there (Fig. 1b). Across runs, the trajectory was rotated either −10° or +10° in pseudorandomized fashion to get a total directional sampling resolution of 10° (Fig. 1c and Supplementary Fig. 1). After every three runs (one run block), all trajectory rotations were sampled equally and in a pseudorandomized order (Fig. 1c and Supplementary Fig. 1). These balanced run blocks served as data partitions for later analysis.

Object location memory task. To focus spatial attention on the virtual environment during the fixation task, participants additionally memorized locations of objects within the arena. Each object was a colored circle (green, red, blue or purple) that was visible only when the fixation target moved across it. After three pseudorandomly chosen trials per run, participants reported the locations of objects by moving a cursor to the memorized location via key presses (one object per cueing, uninformed two-back task, randomly chosen arena orientation), after which the true location was revealed (feedback). Additional feedback about task performance was given in written form at the end of each run to enhance motivation. Two of the objects were positioned at polar coordinates 120° and 300° (0 modulo 60° relative to screen horizontal) and two other objects were at 30° and 210° (30 modulo 60° relative to screen horizontal; Fig. 1c and Supplementary Figs. 1 and 2). Object positions were chosen to ensure that the overlap with the trajectory was balanced across trajectory rotations. Each two-piece set of objects was hence presented equally often and long (0.27 s/trial) regardless of trajectory rotation and did not induce hexadirectional biases. In both viewing and navigation tasks, participants were able to report the locations of the objects (Supplementary Fig. 2d), and there were no differences in spatial memory performance (Euclidean distance between true and memorized location) between objects in either of the tasks (repeated-measures ANOVA results: viewing task: $F_{3,81} = 0.64$, $P = 0.593$;

navigation task: $F_{3,81} = 1.9$, $P = 0.136$). To examine whether differences in spatial memory between objects were masked by differences in putative grid orientation between participants, we grouped objects into aligned and misaligned objects according to their position on each participant's putative grid pattern for each of the arena orientations. We then tested whether spatial memory performance differed between aligned and misaligned objects (averaged across arena orientations) but did not find evidence for it (two-sided t test results: $t_{27} = 0.097$, $P = 0.924$). In addition, the average hexadirectional signal did not correlate with the participants' average spatial memory performance during subsequent first-person navigation ($r = 0.122$, $P = 0.537$). One participant did not finish the final navigation task and was excluded here.

Visual motion control. To test whether entorhinal cortex generally responded to eye movements in our task irrespective of direction, we additionally scanned a control condition in which the fixation target remained in the screen center while the arena moved instead (visual motion control). If entorhinal cortex responded to eye movements, we expected to find an increased activation in the main experiment relative to this control condition since the two conditions only differed in eye movements, not in directional or positional sampling or in otherwise confounding retinal motion. Pixels leaving the screen on one side entered the screen on the other side, keeping visual motion constant over time (Supplementary Fig. 2b) and allowing us to apply the same motion stimulus to the retina in both presence and absence of eye movements. To reserve the major part of scanning time for the main experiment, this control condition was tested only for ~30 s per trial (compared to ~60 s for the main experiment; the same directions were tested, but only once instead of twice). Data was analyzed using a separate first-level general linear model, modeling all onsets of eye or arena movements irrespective of direction or arena orientation. The numbers of onsets of eye movements was downsampled to match the numbers of onsets of the visual motion control. As done for the main analysis, each run was modeled separately and the same nuisance regressors were included. Beta estimates for eye-movement and visual-motion regressors were contrasted for each participant and tested in an ROI-based analysis using two-sided Wilcoxon signed-rank tests (EC: $z = 1.5$, $P = 0.133$; early visual cortex: $z = 4.55$, $P = 5.3 \times 10^{-6}$; motor cortex: $z = -0.08$, $P = 0.940$; frontal lobe: $z = 0.96$, $P = 0.336$; parietal cortex: $z = -2.82$, $P = 4.8 \times 10^{-3}$). If the EC was hexadirectionally modulated in the visual motion control, we expected to find at least a statistical trend despite shorter scanning time. However, we did not find any evidence that the EC was hexadirectionally modulated in our visual motion control (one-sided Wilcoxon signed-rank test results: $z = -0.39$, $P = 0.651$) and both the mean (mean: -8.5×10^{-4}, sem: 0.023) and the median (median: -5.2×10^{-3}, 25th percentile: -0.056, 75th percentile: 0.107) of the aligned versus misaligned contrast were slightly negative.

Data acquisition and preprocessing. Functional T2*-weighted gradient-echo echoplanar images were acquired on a Magnetom PrismaFit 3 Tesla magnetic resonance tomograph with the following parameters: repetition time (TR) = 1,000 ms, echo time (TE) = 34 ms, multiband acceleration factor = 6, voxel size = 2 × 2 × 2 mm, flip angle = 60°, field of view = 210 × 210 mm, 66 slices, base resolution 104 × 104 mm. In addition, an anatomical scan was recorded using a T1-weighed MPRAGE sequence with voxel size 1 × 1 × 1 mm. Functional images were preprocessed using SPM12. Images were corrected for head movements, co-registered to the structural T1 image, spatially normalized to MNI space and smoothed with a 4 mm full-width-at-half-maximum Gaussian kernel.

Regions of interest (ROI) definition. Because the mediotemporal lobe is difficult to image due to magnetic field distortions and susceptibility artifacts, we delineated the EC bilaterally for each individual participant based on the normalized mean-EPI-image using itk-SNAP (http://www.itksnap.org) and carefully double-checked voxel selection with the structural T1 image. This ensured that only voxels belonging to the EC on the functional images were included in the analysis (Supplementary Fig. 3). On average, EC was centered at −18/−12/−25 and included 105 voxels in the left hemisphere and centered at +19/−12/−24 with 106 voxels in the right hemisphere. Hemispheres were combined into one bilateral entorhinal ROI. As control ROIs we chose early visual cortex and motor cortex, for which, to our knowledge, no hexadirectional coding has been reported; the frontal lobe, parts of which exhibit hexadirectional signals[8]; and the parietal cortex, due to its strong involvement in visuospatial processing[14,15]. ROIs were created by co-registering corresponding probability maps of the SPM anatomy toolbox to the structural scan of each participant and thresholding them at 50% probability. The resulting binary masks were of following size: visual cortex: 2,731 voxels, motor cortex: 797 voxels, frontal lobe: 2,780 voxels, parietal lobe: 1,165 voxels. Out-of-brain voxels were neglected. To ensure that potential hexadirectional signals were not washed out due to bigger ROI sizes for control regions compared to the EC, we repeated our main analysis with higher probability thresholds for the control regions (Supplementary Fig. 6). Here thresholds were chosen so that the resulting ROI masks approximated the average size of the EC (211 voxels). Note that the higher-threshold masks comprised voxels with highest probability for belonging to the respective areas; they did not, however, capture the actual extent of the control areas we were interested in. Thresholds and average numbers of voxels were as

follows: visual cortex: 76%, 219 voxels; motor cortex: 69%, 202 voxels; frontal lobe: 99%, 283 voxels; parietal cortex: 84%, 205 voxels. All ROI masks were resliced to match our functional image dimensions.

First-level analysis. Beta coefficients for every direction and voxel were estimated using one mass univariate general linear model per participant. We modeled each movement direction of the fixation target separately for each condition, arena orientation and run with a separate boxcar regressor. Four additional regressors per run modeled (i) presentation of objects, (ii) cueing, (iii) periods during which the fixation target/arena remained stationary and (iv) periods during which behavioral responses were given. Regressors were convolved with the hemodynamic response function. Realignment parameters (translations of X, Y and Z coordinates; pitch, roll and yaw) were modeled as nuisance regressors. Slow signal drifts were removed using a high-pass cutoff filter of 100 Hz and only voxels in gray matter and white matter were included in the analysis.

Hexadirectional analysis. We extracted first-level beta estimates for three data partitions (run blocks), representing the first three, intermediate three and last three runs of the experiment. Within each data partition, all directions were sampled equally while condition sequence (main and control conditions) was counterbalanced, and object presentations, arena orientations and the temporal sequence of trajectory rotations across runs were pseudorandomized. We extracted beta estimates for voxels in the entorhinal cortex, normalized each beta estimate by subtracting the mean across all beta estimates obtained from the same run (to compensate for potential differences in overall beta-estimate amplitude for task regressors between runs) and averaged two of the three data partitions to increase the signal to noise ratio. We then fitted another linear model incorporating two regressors modeling sine and cosine across directions (θ) with 60° periodicity ($\sin(6\theta)$ and $\cos(6\theta)$) as well as one regressor for the grand mean to this 'training set'. The resulting beta estimates for sine ($\beta \sin$) and cosine ($\beta \cos$) of viewing direction were then used to estimate the putative grid orientation (ϕ), or the phase of the oscillatory modulation across directions, as in

$$\varphi = \frac{\arctan\left(\frac{\beta \sin}{\beta \cos}\right)}{6}$$

The third data partition served as the 'test set' and was used to contrast directions aligned (0 modulo 60°) versus misaligned (30 modulo 60°) relative to the estimated putative grid orientation in 20° bins. This process was iterated until each data partition served as test set once and as training set twice. Since directions were sampled in steps of 10°, estimated putative grid orientations would always fall between two actually sampled directions. The 20° bin size was chosen by taking both directions closest to the estimated putative grid orientation (rounded up and down to closest sampled directions). The resulting contrast coefficients were then transformed to z-scores as follows. In each iteration, we bootstrapped the null distribution for each voxel and data partition by shuffling the direction labels of the test set 1,000 times, each time contrasting aligned versus misaligned directions as described before. The training set was not shuffled. We calculated the mean (x) and s.d. (σ) of the null distribution and used it to transform the contrast coefficient (β) to a z-score (z) as in

$$z = \frac{\beta - x}{\sigma}$$

We then averaged the three resulting z-scores of each voxel across the three test sets to obtain one threefold cross-validated z-score per voxel (Supplementary Fig. 4). By averaging these z-scores across arena orientations and voxels of an ROI, we obtained one z-score per participant that was taken to group level. The distribution of z-scores was non-normal (one-sample Kolmogorov–Smirnov goodness-of-fit tests for EC and sixfold rotational symmetry: $K = 0.367$, $P = 5.2 \times 10^{-4}$). To assess statistical significance, we therefore report Wilcoxon signed-rank tests throughout the imaging analysis. The putative grid orientation represents one of the directions for which the fMRI signal is strongest (one of the putative six high peaks across directions). We then contrasted all directions falling on high peaks against all directions falling on low peaks of the putative six-peaked modulation (Fig. 1a). If there is hexadirectional modulation, this contrast should yield positive values independently from the absolute putative grid orientation observed. Note that our main hypothesis is therefore inherently one-sided. We next re-examined the main effect on group level using a nonparametric permutation-based one-sample t test using 10,000 permutations. For each permutation, the signs of the group-level means were switched randomly, each time computing the t score of the permuted data and finally computing the P value for the observed t score based on the resulting t score distribution. The test confirmed previous tests in suggesting significant hexadirectional modulation of the EC ($t_{28} = 2.36$, $P = 0.0126$). Note that even though our analysis should be more conservative when performed on z-scores, it yielded similar results when performed on cross-validated contrast coefficients averaged across voxels before bootstrapping (Fig. 2c and Supplementary Fig. 5). Even though we did observe clustering of putative grid orientations across voxels, our analysis does not rely on such clustering. While

earlier approaches tested putative grid orientations on the ROI level[8], we estimated and tested putative grid orientations for each voxel separately and averaged the resulting z-scores. This way, we maximized sensitivity and increased robustness compared to previous approaches investigating hexadirectional modulation[8]. Since previous studies report stronger hexadirectional signals in right-hemispheric compared to left-hemispheric EC[8,9], we repeated the main analysis for the EC on individual hemispheres (Supplementary Fig. 4). In line with previous reports, right-hemispheric EC elicited strong hexadirectional signals ($z = 2.85$, $P = 2.2 \times 10^{-3}$), while the left-hemispheric EC did not ($z = 1.06$, $P = 0.145$, one-sided Wilcoxon signed-rank test).

Matched ROI sizes. To ensure that potential hexadirectional signals were not washed out due to bigger ROI sizes for control regions compared to the entorhinal cortex, we repeated the analysis for control regions that were matched in size (see above). Again, neither early visual cortex ($z = -0.39$, $P = 0.651$), motor cortex ($z = -0.49$, $P = 0.687$) nor parietal cortex ($z = 1.09$, $P = 0.137$) showed any significant modulation. However, we did observe a weak hexadirectional signal in the frontal lobe ($z = 1.92$, $P = 0.027$), which did not survive Bonferroni correction (Supplementary Fig. 6b). The higher-threshold mask for frontal lobe contained voxels of the prefrontal cortex (PFC; Supplementary Fig. 6a), in a subset of which hexadirectional modulation has been observed previously[8,9]. The weak hexadirectional modulation we observe parallels previous reports of hexadirectional modulation of the PFC.

Examination of putative grid orientations. To see how much orientation estimates varied across voxels in our data, we averaged beta estimates for each direction across the three normalized data partitions (to increase the signal-to-noise ratio) and estimated one putative grid orientation for every voxel with 10° resolution in 60° space (36 bins). We then calculated the circular distance between the orientation estimated for each voxel and the mean orientation across voxels. If putative grid orientations were random across voxels, we would expect a uniform distribution of circular distances around the unit circle. However, if there was a within-participant clustering of putative grid orientations, we should also be able to detect it here across participants as the average putative grid orientation of each participant was set to zero in this test. A V-test for nonuniformity revealed that circular distances were not random across voxels but did indeed cluster around each participant's mean orientation ($V = 31.80$, $P = 3.46 \times 10^{-6}$). Next, we examined whether there was a relationship between the amplitude of the hexadirectional signal of a voxel and the putative grid orientation that was estimated for it. We calculated the circular variance across putative grid orientations for two voxel selections, the strongest 10% and weakest 10% of hexadirectionally modulated voxels of each participant, and found that stronger voxels had a more similar putative grid orientations (smaller across-voxel variances in putative grid orientations) than weaker voxels (one-sided t test results: $t_{28} = -6.67$ $P = 1.5 \times 10^{-7}$, CI [–Inf, –0.19]; Supplementary Fig. 7). To ensure that this clustering did not reflect dependencies introduced by data smoothing, we repeated the analysis using unsmoothed data. Again, the strongest 10% of voxels were more similar in putative grid orientation than the weakest 10% ($t_{28} = -2.74$, $P = 5.3 \times 10^{-3}$, CI [–Inf, –0.02]; Supplementary Fig. 7). To examine whether voxels in one hemisphere were more similar in their putative grid orientation than voxels in different hemispheres, we then used unsmoothed data to compare the average absolute angular differences between putative grid orientations of each voxel to all voxels in the same hemisphere and to all voxels in the other hemisphere. We found that voxels in the same hemisphere had more similar putative grid orientations than voxels in different hemispheres (two-sided t test results: $t_{28} = -3.67$, $P = 0.001$, CI [–0.03, –0.01]). To investigate a potential anchoring of putative grid orientations to perceptual features such as landmarks or screen axes, we then used the strongest 10% of voxels to compute one average putative grid orientation per participant, as described above, using smoothed data. Potential clustering was tested for each arena orientation separately using Rayleigh's tests for nonuniformity, which did not reveal any clustering of putative grid orientations across participants (arena orientation 1: $z = 0.083$, $P = 0.922$; orientation 2: $z = 0.141$, $P = 0.871$).

Eye tracking. Left eye position as well as pupil size was monitored at 1,000 Hz using a video-based infrared eye tracker (Eyelink 1000) with MR-compatible long range optics (for five participants eye tracking calibration failed and no eye tracking was recorded due to technical problems; the imaging main effect (Fig. 2a) remains significant without these participants: aligned vs. misaligned directions: $z = 2.16$, $P = 0.016$). Eye tracking data (Supplementary Fig. 8) was linearly detrended and smoothed with a running average kernel of 100 ms. To additionally compensate for slow signal drifts, the across-trial median x and y positions were set to zero for both gaze and the fixation target. Data was downsampled to the monitor refresh rate of 60 Hz. Noise due to lost tracking or blinks was discarded by removing any samples for which pupil size deviated more than one s.d. from the mean across the time series. We then calculated the across-trial average Euclidean distance between fixation target and gaze position for each direction (fixation error). Since a repeated-measures ANOVA revealed differences in fixation error between directions ($F_{35, 805} = 8.57$, $P = 3.5 \times 10^{-36}$), we used an approach similar to that used in the imaging data analysis to test for potential symmetries of this effect.

We fitted regressors for sine and cosine of eye movement direction for four-, five-, six-, seven- and eightfold rotational symmetry (plus constant term) to the fixation error across directions of each participant. We then performed another repeated-measures ANOVA to test for differences in the R^2 statistics of these models and did not find any difference produced by different symmetries ($F_{4,92} = 1.7$, $P = 0.156$). Differences in fixation accuracy therefore cannot explain our imaging results. The average fixation error of each participant differed between the main experiment and visual motion control (two-sided t test results: $t_{23} = 12.65$, $P = 7.6 \times 10^{-12}$, CI [0.79, 1.10]), which was expected given that the fixation target moved in the main experiment but not in the visual motion control. Participants with higher fixation errors in the main experiment also showed higher fixation errors in the visual motion control, which might reflect general differences across participants in target tracking ability, but could also reflect differences in eye tracking quality between participants. For five participants, fixation errors in the main experiment were higher than 1 s.d. from the mean across participants, indicating poor tracking performance. These participants were excluded from imaging analysis. In addition to fixation error, we calculated the average eye movement velocity for all 36 directions and tested for differences with repeated-measures ANOVA but did not find any differences ($F_{35,805} = 1.1$, $P = 0.313$). The average eye velocity matched that of the fixation target (average eye velocity across participants: 7.75 ± 0.183 °/s, constant velocity of fixation target: 7.5°/s). Taken together, these results are not suggestive of any hexadirectional biases and show that participants performed the visual tracking task.

Life Sciences Reporting Summary. Further information on experimental design is available in the Life Sciences Reporting Summary.

Data and code availability. The data that support the findings of this study and the analysis code are available from the corresponding author upon reasonable request.

natureresearch

Corresponding author(s):   Matthias Nau, Christian F. Doeller

☐ Initial submission   ☐ Revised version   ☒ Final submission

Life Sciences Reporting Summary

Nature Research wishes to improve the reproducibility of the work that we publish. This form is intended for publication with all accepted life science papers and provides structure for consistency and transparency in reporting. Every life science submission will use this form; some list items might not apply to an individual manuscript, but all fields must be completed for clarity.

For further information on the points included in this form, see Reporting Life Sciences Research. For further information on Nature Research policies, including our data availability policy, see Authors & Referees and the Editorial Policy Checklist.

▶ Experimental design

1. Sample size

Describe how sample size was determined.

One-sided hypothesis for hexadirectional signal in EC.

Apriori G*Power analysis for 80% power, alpha 0.05, assumed medium effect size: d=0.5. Total sample size of n = 27.

We scanned 36 participants accounting for potential drop-outs. In total, 29 participants entered the analysis.

2. Data exclusions

Describe any data exclusions.

Strong head movements during scanning (n=2), by visual examination frequently larger than voxel size of 2x2x2mm.

Fixation error higher than one standard deviation above the mean across participants (n=5, see Online Methods: 'Participants')

3. Replication

Describe whether the experimental findings were reliably reproduced.

One fMRI study was conducted and replication was not attempted.

4. Randomization

Describe how samples/organisms/participants were allocated into experimental groups.

Participants were not grouped and hence no randomization was performed.

See Online Methods, paragraph: 'Participants'

5. Blinding

Describe whether the investigators were blinded to group allocation during data collection and/or analysis.

Participants were not grouped and hence no blinding procedure was performed.

See Online Methods, paragraph: 'Participants'

Note: all studies involving animals and/or human research participants must disclose whether blinding and randomization were used.

6. Statistical parameters

For all figures and tables that use statistical methods, confirm that the following items are present in relevant figure legends (or in the Methods section if additional space is needed).

n/a	Confirmed	
☐	☒	The <u>exact sample size</u> (*n*) for each experimental group/condition, given as a discrete number and unit of measurement (animals, litters, cultures, etc.)
☐	☒	A description of how samples were collected, noting whether measurements were taken from distinct samples or whether the same sample was measured repeatedly
☐	☒	A statement indicating how many times each experiment was replicated
☐	☒	The statistical test(s) used and whether they are one- or two-sided (note: only common tests should be described solely by name; more complex techniques should be described in the Methods section)
☐	☒	A description of any assumptions or corrections, such as an adjustment for multiple comparisons
☐	☒	The test results (e.g. *P* values) given as exact values whenever possible and with confidence intervals noted
☐	☒	A clear description of statistics including <u>central tendency</u> (e.g. median, mean) and <u>variation</u> (e.g. standard deviation, interquartile range)
☐	☒	Clearly defined error bars

See the web collection on statistics for biologists for further resources and guidance.

▶ Software

7. Software

Describe the software used to analyze the data in this study.

> Virtual environment was created and presented using UnrealEngine2 (https://www.unrealengine.com/)
>
> Viewing task was created and presented using Psychophysics Toolbox Version 3 (http://psychtoolbox.org/) running on Matlab2016 (https://se.mathworks.com/).
>
> MRI data was analyzed using SPM12 and Matlab2016 (https://se.mathworks.com/). Statistical tests involved Circular Statistics Toolbox (P. Berens, CircStat: A Matlab Toolbox for Circular Statistics, Journal of Statistical Software, Volume 31, Issue 10, 2009).

For manuscripts utilizing custom algorithms or software that are central to the paper but not yet described in the published literature, software must be made available to editors and reviewers upon request. We strongly encourage code deposition in a community repository (e.g. GitHub). *Nature Methods* guidance for providing algorithms and software for publication provides further information on this topic.

▶ Materials and reagents

8. Materials availability

Indicate whether there are restrictions on availability of unique materials or if these materials are only available for distribution by a for-profit company.

> No unique materials were used

9. Antibodies

Describe the antibodies used and how they were validated for use in the system under study (i.e. assay and species).

> No antibodies were used

10. Eukaryotic cell lines

a. State the source of each eukaryotic cell line used.

> No cell lines were used

b. Describe the method of cell line authentication used.

> No cell lines were used

c. Report whether the cell lines were tested for mycoplasma contamination.

> No cell lines were used

d. If any of the cell lines used are listed in the database of commonly misidentified cell lines maintained by ICLAC, provide a scientific rationale for their use.

> No cell lines were used

▶ Animals and human research participants

11. Description of research animals

Provide details on animals and/or animal-derived materials used in the study.

> No animals were tested

12. Description of human research participants

Describe the covariate-relevant population characteristics of the human research participants.

> A total of 36 participants (22 female, age range: 18-35, normal or corrected to normal vision) were recruited for this study via the Radboud University Nijmegen online recruitment system. In total, 29 participants entered the analysis.
>
> See Online Methods, paragraph 'Participants'

nature research

Corresponding author(s):   Matthias Nau, Christian F. Doeller

☐ Initial submission ☐ Revised version ☒ Final submission

MRI Studies Reporting Summary

Form fields will expand as needed. Please do not leave fields blank.

▶ Experimental design

1. Describe the experimental design.

   Task fMRI with event-related design

2. Specify the number of blocks, trials or experimental units per session and/or subject, and specify the length of each trial or block (if trials are blocked) and interval between trials.

   9 runs with 9 trials each were scanned per participant. Each trial lasted ~1 minute and tested a set of 12 movement directions twice in blocks of 2 seconds per direction. Directions were sampled twice per trial and in sequences which were 3-5 directions in length (2x3, 2x4, 2x5 = 2 x 12 = 24 directions). After each of these sequences the fixation target stopped for 1 second, jumped to another pseudorandomly chosen position, remained stationary for 1.5 seconds and continued moving from there until every direction was sampled twice. After 3 pseudorandomly chosen trials participants gave behavioral responses after which the next trial was started.

3. Describe how behavioral performance was measured.

   Visual tracking task: Eye tracking monitored fixation error (average Euclidean distance between target and gaze location) across eye movement directions which were tested with repeated measures ANOVA on group level.

   Object location memory task: Participants reported memorized locations by moving a cursor and logging memorized location. Average Euclidean distance between logged and true location was tested with repeated measures ANOVA on group level.

▶ Acquisition

4. Imaging

   a. Specify the type(s) of imaging.

   Functional

   b. Specify the field strength (in Tesla).

   3 Tesla

   c. Provide the essential sequence imaging parameters.

   Functional T2*-weighted gradient-echo echoplanar images with following parameters: repetition time (TR) = 1000ms, echo time (TE) = 34 ms, multiband acceleration factor 6, voxel size 2x2x2mm, flip angle 60°, field of view 210x210 mm, 66 slices, base resolution 104 x104 mm. Anatomical scan was recorded using a T1-weighed MPRAGE sequence with voxel size 1x1x1 mm.

   d. For diffusion MRI, provide full details of imaging parameters.

   N/A

5. State area of acquisition.

   Whole-brain

▶ Preprocessing

6. Describe the software used for preprocessing.

   Functional images were preprocessed using SPM12 in Matlab 2016. Images were realigned, co-registered to the structural T1-image, spatially normalized to MNI space and smoothed with a 4mm full-width-at-half-maximum Gaussian kernel.

7. Normalization

    a. If data were normalized/standardized, describe the approach(es).

> Functional and structural images were normalized to MNI space using a 12-parameter affine transformation and non-linear transformation in SPM12.

    b. Describe the template used for normalization/ transformation.

> ICBM space template - European brains

8. Describe your procedure for artifact and structured noise removal.

> Realignment parameters were modeled as nuisance regressors. First-level analysis was masked with participant-specific implicit mask. Implicit mask was obtained by combining probability masks for gray- and white matter obtained in brain segmentation step performed in SPM12. Probability masks were smoothed with a 2x2x2mm FWHM-Gaussian kernel to compensate for small distortion effects.

9. Define your software and/or method and criteria for volume censoring, and state the extent of such censoring.

> No volume censoring was performed.

▸ Statistical modeling & inference

10. Define your model type and settings.

> In this study, participants were fixating at a moving fixation target. We modeled twelve movement directions separately for two conditions, two arena orientation and nine runs with a separate boxcar regressor in one mass univariate general linear model per participant. Four additional regressors per run modeled 1) presentation of objects, 2) cueing, 3) periods when the fixation target remained stationary- and 4) periods when behavioral responses were given (button presses). Regressors were convolved with the hemodynamic response function. Realignment parameters (translations of X, Y, and Z coordinates, pitch, roll, and yaw) were modeled as nuisance regressors. Slow signal drifts were removed using a high-pass cutoff filter of 100 Hz and only voxels in gray matter and white matter entered analysis (implicit masking).

11. Specify the precise effect tested.

> We estimated the phase of a 6-peaked oscillatory modulation across directions for every voxel in an iterative three-fold cross-validation procedure (see Online Methods) and contrasted directions in 60° steps relative to this estimated phase ('aligned directions', 0 modulo 60°) versus directions in 60°-steps with 30° phase-shift ('misaligned directions', 30 modulo 60°) in 20° bins. We then transformed the resulting contrast coefficients into z-scores in a bootstrapping procedure (shuffling direction labels of our data 1000 times for each voxel). For each participants, we then averaged the resulting z-scores across the three iterations and across voxels of an ROI and took the resulting contrast coefficient to the group level. We performed a one-sided Wilcoxon signed rank tests to test whether aligned directions elicited stronger responses than misaligned directions (consistently across participants).

12. Analysis

    a. Specify whether analysis is whole brain or ROI-based.

> ROI-based

    b. If ROI-based, describe how anatomical locations were determined.

> EC was delineated bilaterally for each individual participant based on the normalized mean-EPI-image using itk-SNAP (http://www.itksnap.org). Voxel-selection was carefully double-checked with structural T1-image. Hemispheres were combined to one bilateral entorhinal ROI. ROIs for primary visual cortex, motor cortex, parietal cortex and frontal lobe were created by thresholding corresponding probability maps of the SPM anatomy toolbox at 50%. The resulting binary masks were coregistered to the structural scan of each participant.

13. State the statistic type for inference.
    (See Eklund et al. 2016.)

Voxel-wise tests were performed in a iterative three-fold cross-validation procedure (see Online Methods). The results were averaged across iterations and voxels within an ROI to obtain one z-score (contrast) per participant that was taken to the group level and tested against zero with a one-sided Wilcoxon signed rank test.

14. Describe the type of correction and how it is obtained for multiple comparisons.

Bonferroni correction

15. Connectivity

    a. For functional and/or effective connectivity, report the measures of dependence used and the model details.

N/A

    b. For graph analysis, report the dependent variable and functional connectivity measure.

N/A

16. For multivariate modeling and predictive analysis, specify independent variables, features extraction and dimension reduction, model, training and evaluation metrics.

N/A